Comparative Investigation of Red and Orange Roman Tesserae: Role of Cu and Pb in Colour Formation

Cecile Noirot, Laurent Cormier, Nadine Schibille, Nicolas F Menguy, Nicolas Trcera, Emiliano Fonda

heritage

MDPI

Article

Comparative Investigation of Red and Orange Roman Tesserae: Role of Cu and Pb in Colour Formation

Cécile Noirot [1], Laurent Cormier [1,*], Nadine Schibille [2], Nicolas Menguy [1], Nicolas Trcera [3] and Emiliano Fonda [3]

[1] Institut de Minéralogie de Physique des Matériaux et de Cosmochimie (IMPMC), Sorbonne Université, CNRS UMR7590, MNHN, IRD, 4 Place Jussieu, 75005 Paris, France
[2] IRAMAT-CEB, UMR7065, CNRS/Université d'Orléans, 3D rue de la Férollerie, CS 60061, CEDEX 2, 45071 Orleans, France
[3] Synchrotron SOLEIL, L'Orme des Merisiers, Saint Aubin BP48, CEDEX, 91192 Gif sur Yvette, France
* Correspondence: laurent.cormier@sorbonne-universite.fr

Abstract: This study aims at the characterisation of red and orange glass tesserae from the 4th-century Roman villa of Noheda (Spain). Due to the limited number of analyses available for such ancient materials, many questions remain unanswered about the production processes in the Roman period. Six samples were chosen for their hue variations, including two samples showing banded patterns of red and orange. Differences in copper speciation were investigated by X-ray absorption spectroscopy and compared with colour and compositional variations obtained by EPMA. The shapes and sizes of colouring crystals could be investigated using scanning and transmission electron microscope imaging. The brown-red colour is due to metallic copper nano-particles and corresponds to a low-copper and low-lead group usually described in the literature. The orange samples and bands are coloured by copper oxide Cu_2O nanoparticles with remaining Cu^+ in the glass and have greater contents of Cu. Compositional analyses reveal that the same base glass is used in the red and orange bands with additions of Cu, Sn, Pb and probable Fe. Furthermore, based on our results and on the literature review, a high-copper low-lead group of glasses highlights the variability of compositions observed in cuprite colours.

Keywords: copper red; glass colouration; Roman glass; nanoparticles; electron microscopy; XANES

Citation: Noirot, C.; Cormier, L.; Schibille, N.; Menguy, N.; Trcera, N.; Fonda, E. Comparative Investigation of Red and Orange Roman Tesserae: Role of Cu and Pb in Colour Formation. *Heritage* **2022**, *5*, 2628–2645. https://doi.org/10.3390/heritage5030137

Academic Editor: Monica Ganio

Received: 29 July 2022
Accepted: 2 September 2022
Published: 9 September 2022

1. Introduction

Ancient glasses coloured by the precipitation of copper have attracted the attention of researchers due to their frequent occurrence but also because they are challenging to produce. The production of red/orange glasses requires excellent control of the melting conditions, in particular the furnace atmosphere, the melting temperature and the cooling treatment, as well as the glass composition with the possible use of reducing agents (Fe, Sb, Sn) and lead. Colourations vary from bright red and brown-red to orange, and the colour quality depends on the size of micrometric or even nanometric crystals that can be either metallic copper or cuprite (Cu_2O). Most studies concerning the synthesis of red colouration using copper have been dedicated to transparent glasses [1–3] or glazes [4–6], while investigations of opaque glasses mainly concern the analysis of ancient samples. Nevertheless, there are a few articles that address the reproduction of opaque glasses: Drünert et al. [7] reproduced German medieval brown glasses coloured by metallic copper particles, and Ahmed and Ashour [8–10] were able to produce orange opaque glasses with dendritic cuprite crystals.

The precipitation of copper as a colouring agent in glasses has been reported as early as the mid 15th century BCE as glass beads and amulets in Mesopotamia [11,12], and since the mid 14th century BCE in Egypt [12]. Since then, copper red has been found in numerous areas and various time periods. Orange and red glass beads from the 5th–1st

centuries BCE have been reported in South Asia (India, Thailand, and Sri Lanka) [13–15], with both Cu_2O and Cu^0 colourations. Cuprite red was also very popular in enamel work in the Celtic period (4th–1st century BCE) [16] and the early Middle Ages in Europe [17]. Roman mosaic tesserae and glass sectilias (4th century BCE-4th century CE) have been extensively studied, mostly from sites in Italy [12,18–23] but also from other parts of the Roman Empire (Gallo-Roman and Hispano-Roman glasses) [16,24]. Both red and orange colours are observed in these mosaics, and copper is found as metallic precipitates or Cu_2O crystals. Early Christian and Byzantine mosaics still use red glass tesserae [16,24–28]. In medieval Europe (12th–16th century CE), copper red was mainly used for stained glass windows as a thin layer on top of or sandwiched between layers of uncoloured glass [29,30]. Colouration of glazes on ceramics by metallic copper nano-particles can be traced back to the Chinese Tang dynasty (7th–10th century CE) [31] and experienced a revival in China in the 18th century, as well as in Europe through Orientalism [32]. Before the 17th century CE, virtually all red glasses were coloured by copper, with only a few exceptions such as the Lycurgus Cup, coloured by silver-gold alloy nano-particles [12].

Currently, copper red in stained glass windows, transparent objects and ceramic glazes is only used in artisanal and artistic productions due to the challenge of controlling the final product, which makes it a costly material as a good achievement is not guaranteed. In industrial productions, cheaper but more toxic Cd(S,Se) pigments are preferred, but they produce vivid, transparent orange and red hues. All modern copper reds are coloured by metallic copper nanoparticles, unlike ancient samples in which occurrences of cuprite are common.

In this study, tesserae from the Roman villa of Noheda (Cuenca, Spain, dated to the 4th century CE) are analysed, focusing on the microstructure of the colouring pigments. The base glass characteristics and possible provenance of the mosaic tesserae from Noheda have been discussed in detail in an earlier publication [24]. The site is remarkable because it hosts one of the largest floor mosaics found from the Roman period, displaying mythological scenes and containing numerous red and orange glass tesserae. Samples in this study were selected for their colour variations and texture. Indeed, Roman tesserae often show non-homogeneous colours, with streaks or even stripes of various hues of red, orange and colourless glasses [18,20–23]. Streaks are also observed in early Christian and Byzantine glass tesserae [26,27] and early Anglo-Saxon glass beads [33]. This aspect of colour texture has been poorly investigated, even though it can shed new light on glass making processes and techniques, including redox control during firing. This study investigates the colour heterogeneity in opaque red and orange glasses and its links with glass composition and copper precipitation. This can help decipher what technology was mastered in the Roman world in the 4th century.

2. Materials and Methods

2.1. Samples Desciption

Six glass tesserae from the Roman villa of Noheda (Spain), dated from the fourth century, were selected from a batch of seventy-four different red and orange tesserae. The selection covers the whole range of orange (samples 70 and 66) to "sealing wax red" (samples 14 and 29), as well as striated samples (25 and 62) showing alternated orange and red stripes. The presence of more than one colour in the same sample could reveal information on the manufacturing processes. Chemical compositions using LA-ICP-MS analysis were previously published [24]. Four of the tesserae are natron-type glasses (14, 29, 66, 70), while the two striated tesserae (25, 62) have magnesium and potassium oxide in excess of 1.5%, suggesting the incorporation of plant ash [34]. All the glasses have a relatively high Fe content, while the orange tesserae have additionally high Cu and Pb concentrations. The selected samples were cut in the middle and the cross-sections were polished down to 1/4 micron diamond paste. The samples are shown in Figure 1.

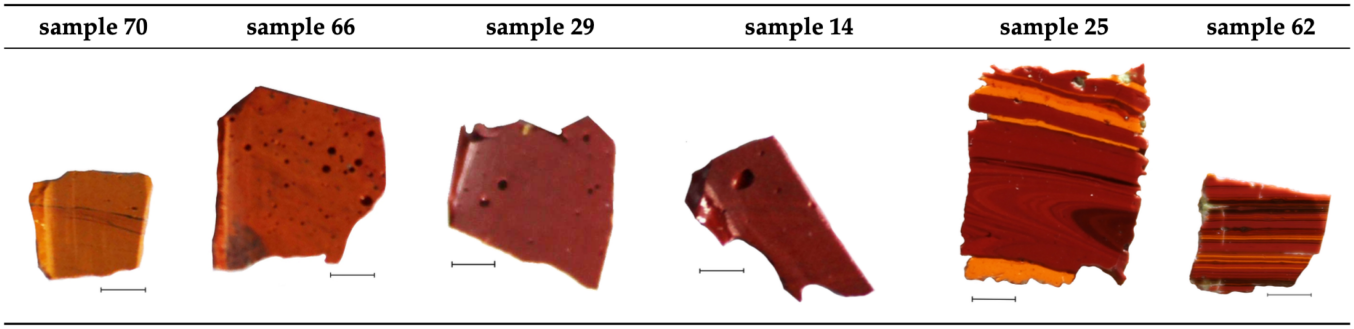

Figure 1. Photos of the studied samples. All scale bars correspond to 2 mm.

2.2. Composition Analyses

Quantitative elemental analysis were performed using a Cameca SX100 electron probe micro analyser (EPMA) at the CAMPARIS facility (Sorbonne Université, Paris, France), equipped with 5 wavelength-dispersive spectrometers. The energy resolution of the spectrometers is sufficient to separate lead M and sulphur K lines. A set of well-characterized minerals were used as standards for calibration. References for the alkali, aluminium and silicon were albite, diopside and orthose. Metallic Cu and SnO_2 are references for Cu and Sn. Other references include $BaSO_4$, MnTi and PbS. Operating conditions for line scans and point analysis were: accelerating potential 15 kV, beam current 10 nA and beam size 20 µm, with limited counting time to limit the alkali migration and at the same time small enough to study composition variations across stripes.

2.3. X-ray Absorption Spectroscopy

XANES (X-ray absorption near edge structure) spectra at the Cu K-edge were recorded on the SAMBA beamline at the Soleil synchrotron facility (Saint-Aubin, France) using a Si(220) double crystal monochromator [35]. Data were collected in total fluorescent yield mode. The beamsize was 300 × 300 $(\mu m)^2$. A Cu metallic foil was used for the energy calibration (first inflection point of the edge set to 8978.9 eV) [36]. The edge energy was determined at the first derivative maximum position of the main absorption edge, and spectra were normalized with linear pre- and post-edge background functions. Finally, spectra were corrected from self-absorption based on the measured composition (EPMA), revealing self-absorption effects for samples 66 and 70 and no effects for samples 14 and 29. All the data analysis was performed using the Athena software [37].

The beam size on SAMBA beamline was too large to discriminate the fine stripes in samples 25 and 62. Evaluation of redox by µ-XANES was thus performed at the Cu $L_{2,3}$-edge on the LUCIA beamline at SOLEIL [38]. The beam size was narrowed down to 5 × 200 $(\mu m)^2$. Striped samples were placed so that the stripes were parallel to this rectangular beam; this way the beam would hit only one colour at a time. A Kohzu five-component double crystal monochromator was used, with total fluorescence yield as detection. The energy was calibrated by setting the edge (derivative of the first maximum) of the XANES spectrum of tenorite CuO to 931.2 eV [39]. The linear pre-edge normalisation function and a three-order polynomial fit on the post-edge area were used. The value of the polynomial fit was fixed at the edge step. Only L_3-edge XANES spectra are presented since they exhibit a better signal/noise ratio than L_2-edge XANES spectra.

2.4. Electronic Imaging

SEM (scanning electron microscope) images were acquired using a Zeiss Ultra 55 field emission gun, at an acceleration voltage of 15 keV. The working distance of 7.5 mm was chosen so that energy dispersive X-ray spectrometry (EDXS) measurements were possible along with imaging. Backscattered electron (AsB, Angle Selective Backscatter electrons) or secondary electron (SE2) detection modes were used to investigate the microstructure. EDXS point analysis was performed using an EDXS QUANTAX system equipped with

a silicon drift detector XFlash 4010 (Bruker). The particle diameter distributions were deduced by a simple threshold treatment in ImageJ, and the mean diameter was taken as the maximum of the histogram. Note that the sizes are given by SEM images, which can cause a slight overestimation due to the electronic interaction volume. The sizes measured here are nonetheless coherent with those of crystals detected by TEM. No additional smaller crystals were observed in TEM, which implies that the surface density of particles determined by SEM imaging is a correct evaluation.

Electron transparent foils were prepared using a focused ion beam (FIB) on a FIB ZEISS Neon 40EsB instrument. FIB sections were analyzed via transmission electron microscopy (TEM) using a JEOL 2100 F Schottky emission gun instrument operating at 200 kV in combination with an UltraScan 4000 Gatan CCD camera and an energy dispersive X-ray detector with 140 eV resolution for elemental mapping. Selected area electron diffraction (SAED) patterns were recorded to identify the structure of the crystals.

3. Results

3.1. Monochrome Tesserae with Orange or Red Colour

3.1.1. XANES Spectra at Cu K-Edge

The Cu K-edge XANES spectra of the monochrome tesserae are shown in Figure 2. The comparison of the spectral features in the near-edge region with those of crystalline compounds provides information on the copper speciation. Five peaks can be distinguished: A (8980 eV), B/B′(8981.6/8983 eV), C (white line, 8994 eV) and D (9002.8 eV). Peaks A and D are characteristic features of metallic copper. Peaks B and B′ correspond to the low-energy pre-edge peak due to $1s \rightarrow 4p$ transitions in Cu(I). The speciation shifts this transition from slightly lower energy (peak B in cuprite) to slightly higher energy (peak B′ for dissolved Cu^{+} ions). Note that peaks A, B and B′ are due to the same $1s \rightarrow 4p$ transition, with different positions indicative of the environment of copper [29,40]. In tenorite (CuO), this transition is further shifted to higher energy values (8986 eV), and this peak position is thus associated with Cu^{2+} species [29].

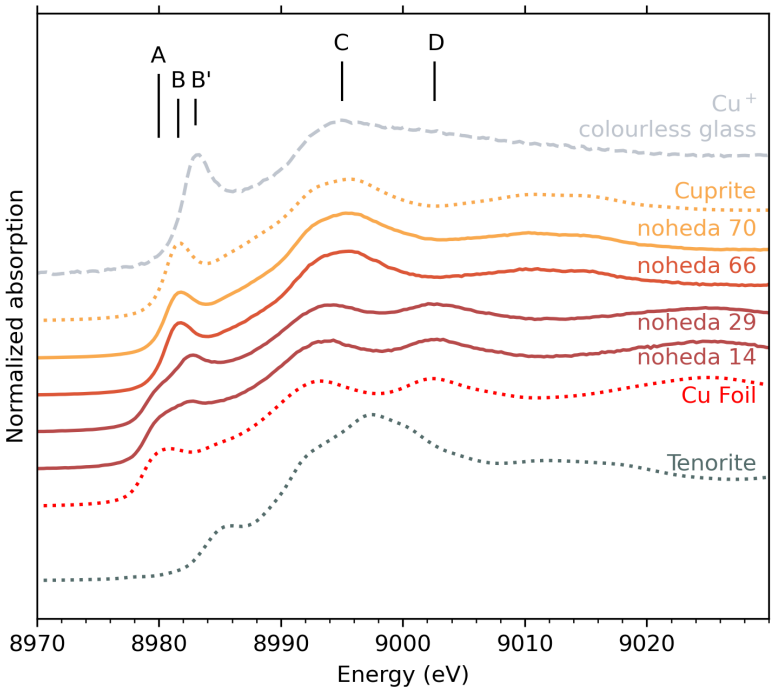

Figure 2. XANES spectra at Cu K-edge of tesserae with orange (Noheda 70 and 66) and red (Noheda 29 and 14) colours, compared with reference material. Vertical shifts were arbitrarily added for better reading.

In the red tesserae (samples 14 and 29), peaks A, C and D are shared with the spectrum of metallic copper, with only a 1 eV blueshift from the bulk copper foil white line (peak C). Peaks A and D in particular indicate the presence of metallic copper (Cu^0) in samples 14 and 29. The presence of peak B′ in red samples reflects the presence of Cu^+ ions, with a larger proportion in sample 29 than in sample 14, indicated by a more pronounced peak.

In contrast, for orange tesserae (samples 66 and 70), only peaks B (8981.6 eV) and C (8995.5 eV blueshifted compared to red samples) are observed. The position and relative intensity of these two peaks match exactly those observed for cuprite Cu_2O. This unambiguously indicates that a large majority of copper ions in these samples are Cu^+ species and that they are located in cuprite crystals. The assignment of red to metallic copper and orange to cuprite is also consistent with X-ray diffraction, as seen in Figure S1.

In order to quantify the different speciations of copper that coexist in the tesserae, fits using linear combination of reference spectra were used. The references used in the fits were metallic copper and cuprite. To account for Cu^+ ions incorporated in the glass (as opposed to a crystalline environment such as cuprite), the spectrum of a transparent glass containing copper was used (Figure 2, top curve). A reference spectrum accounting for Cu^{2+} ions did not improve the fit, which indicates that copper is only found in reduced states. The simulated spectra show good agreement with the experimental spectra, and the results of the fits are presented in Table 1 and Figure S2. For samples 70 and 66, only cuprite is detected. For samples 29 and 14, 75 to 82 % of Cu atoms are located in metallic precipitates, with Cu^+ ions remaining in the glassy matrix.

Table 1. Results of linear combinations used to fit the sample spectrum using reference spectra. R factor of fit represents the goodness-of-fit value, defined as $\frac{\Sigma(data-fit)^2}{\Sigma(data)^2}$. The lower the R value, the better the fit.

	Cuprite	Cu Foil	Cu^+ Colourless Glass	R Factor of Fit
Noheda 70	1	-	-	0.0027
Noheda 66	1	-	-	0.0008
Noheda 29	-	0.75	0.25	0.0013
Noheda 14	-	0.82	0.18	0.0009

3.1.2. Microstructure

SEM images of the orange and red samples (Figure 3) reveal crystals embedded in the glass. The major difference between the orange and red tesserae is the size and the number density of crystals. To compare the size and number of particles, a threshold treatment on the images was performed. In the red sample (n. 29), the crystal diameter varies in the 450–750 nm range, and the surface density of particles is estimated to be 0.06 $particles.\mu m^{-2}$. The orange sample (n. 70) displays crystals with a greater diversity of diameters, ranging from 310 to 750 nm, with additional larger interlaced copper-rich crystals as seen in the center of the image in Figure 3b. The characteristic size for these large crystals is estimated to be around 1 µm. The surface density of particles for sample 70 is evaluated as 0.47 $particles.\mu m^{-2}$, which is almost ten times the number surface density of the red tesserae (n. 29). This surface density of particles excludes the zone with large interlaced crystals. EDX analyses indicate that the dense crystals which appear as white dots on the SEM images in both samples are copper-rich phases. However, this method does not determine whether it is metallic copper or cuprite. For the red and orange tesserae, crystals are heterogeneously distributed. For instance, in the diagonals of the two SEM images, we can see elongated zones with particle depletion. Moreover, EDX analyses reveal that these zones correspond to glasses with lower copper contents compared to the mean composition of the zones that contain particles.

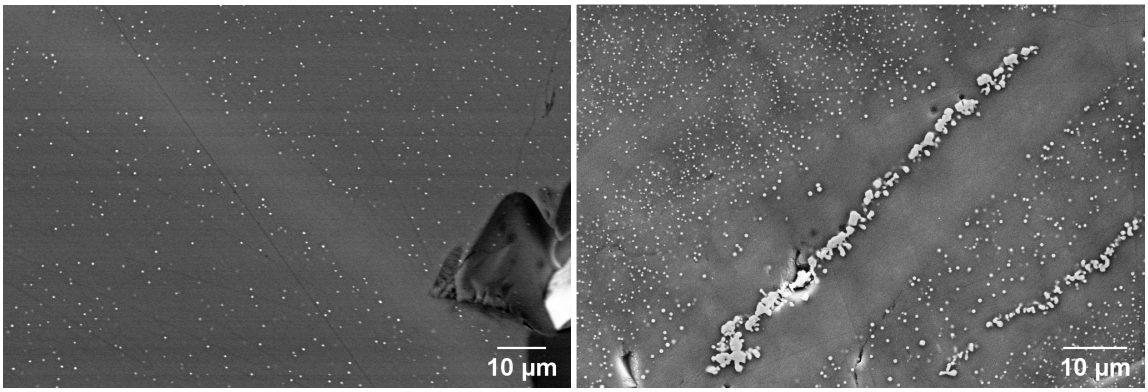

(**a**) (**b**)

Figure 3. SEM imaging of (**a**) red sample 29 in AsB detection and (**b**) orange sample 70 in SE2 detection.

3.2. Striated Tesserae

3.2.1. Chemical Composition Variations

For striped tesserae 25 and 62, composition profiles were measured by EPMA along a line scan crossing the stripes perpendicularly. In Figure 4, the variations in composition along the profiles are plotted, with a picture showing the colour variations as a guide. In both cases, the composition profiles show two main compositions, spatially distributed to form zones of high-lead/high-copper content, alternating with zones having lower lead and copper contents. The zone repartition essentially matches the orange and red stripes, with some exceptions discussed below.

Red stripes roughly correspond to the low-lead/low-copper zones, and the orange stripes are associated with the high-lead/high-copper zones. However, the composition change is insufficient to discriminate chemical evolutions between dark red regions and paler, "wax" red regions. Though less pronounced, the concentrations of other elements also show some variations between the different zones. Compared to the red regions, the orange regions show a trend towards depletion of S, K, Ca and Mg (and possibly Na) and an increase in Fe and Sn.

In sample 25, a more complex behaviour can be observed in a red region located between the depths of 350 and 1380 µm. This zone is distinct from the other red zones described earlier, as it has a low copper, but a high lead content. Surprisingly, no colour contrast is evident in this specific zone compared to the adjacent red area beyond 1380 µm. Rather, an orange to red contrast is observed at 350 µm depth, correlated with the strong change in copper content.

From the EPMA data, the distinctive average compositions of the orange and red zones are determined (Table 2). The zones used to calculate these averaged values are indicated by the vertical dotted lines in Figure 4 delimiting orange and red regions for each sample. Due to the thinness of the orange stripe, the standard variation for the average composition is large. Compared to the red zones, the orange regions are enriched in Cu and Pb and slightly enriched in Sn and Fe.

A base glass composition was calculated for the orange and red regions by subtracting from the composition the copper content and the contents of the additional elements (Pb, Sn, Fe) that are suspected to have been introduced with the copper raw materials or intentionally added to favour crystallization of copper nanoparticles. After normalization to 100 wt%, the base glass compositions are presented in Table 2. They appear remarkably consistent for the two samples and for the red and orange regions, indicating that the same base glass was used. We note only high sulphur contents in the orange part, suggesting its introduction with the colouring raw materials.

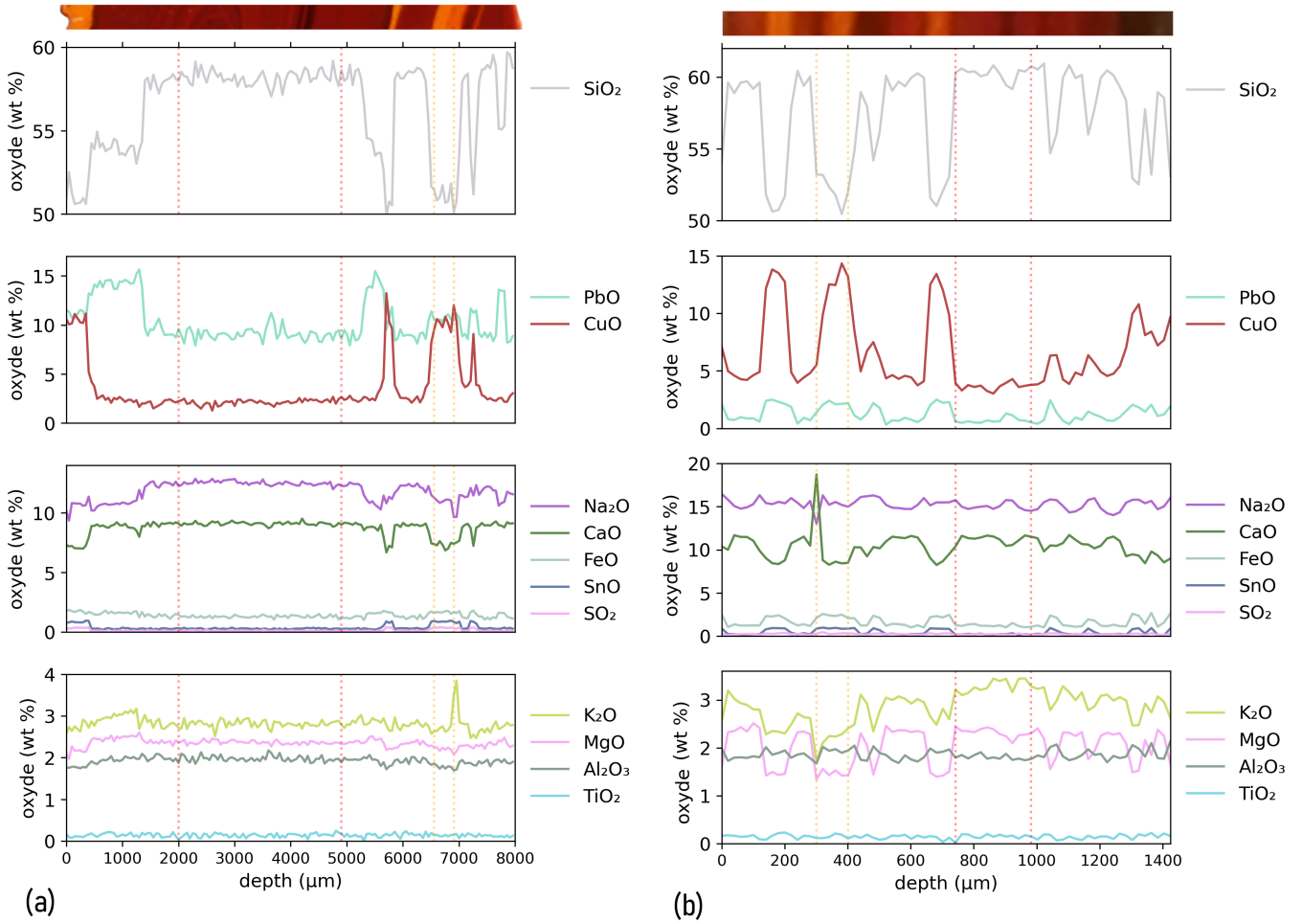

Figure 4. Composition profiles measured by EPMA along the direction perpendicular to the stripes. The coloured band above the graph shows a picture of the analyzed tesserae, with matching depth axis. (**a**) Composition profile for sample 25. (**b**) Composition profile for sample 62.

Table 2. Average composition of the orange and red zones of the striated samples by EPMA. Numbers in parenthesis indicate the uncertainty on the last digit, computed as the standard variation.

Oxide wt%	Na_2O	SiO_2	Al_2O_3	CaO	CuO	SnO	K_2O	MgO	TiO_2	FeO	SO_2	PbO
Sample 25												
Red zones	12.5(2)	58.2(4)	1.98(7)	9.1(1)	2.1(3)	0.29(4)	2.81(8)	2.36(4)	0.14(5)	1.3(1)	0.11(3)	9.1(6)
Base glass	14.3	66.7	2.3	10.4	-	-	3.2	2.7	0.2	-	0.1	-
Orange zones	10.8(7)	51(3)	1.78(9)	7.3(8)	10(3)	0.9(3)	2.8(1)	2.2(1)	0.13(4)	1.6(2)	0.4(1)	10(2)
Base glass	14.1	66.7	2.3	9.6	-	-	3.7	2.9	0.2	-	0.5	-
Sample 62												
Red zones	15.0(4)	60.2(5)	1.80(5)	11.2(4)	3.6(3)	0.20(5)	3.3(1)	2.31(9)	0.15(5)	1.2(1)	0.18(5)	0.7(2)
Base glass	14.3	66.7	2.3	10.4	-	-	3.2	2.7	0.2	-	0.1	-
Orange zones	15(1)	52(1)	1.9(1)	10(4)	11(3)	0.89(5)	2.2(2)	1.45(8)	0.15(4)	2.3(2)	0.31(8)	2.0(3)
Base glass	14.1	66.7	2.3	9.6	-	-	3.7	2.9	0.2	-	0.5	-

Some large inclusions of metallic copper can be observed in the orange region of sample 25, while copper associated with antimony and sulphur was found in one of the red parts of sample 25 (see Figure S3) with sizes of a few micrometers, which is bigger than the copper-suphur phases observed by Bandiera et al. [18]. They are partially dissolved and could be relics of the raw copper materials [23,24].

3.2.2. XANES Spectra at L_3-Edges

XANES spectra at the Cu L_3-edge were obtained on different 5 × 200 $(\mu m)^2$ points in the orange and red parts of the tesserae 25 and 62 (Figure 5). All spectra exhibit a peak A at 931.6 eV and a peak B at 935–935.4 eV, depending on the measured point. Using the attribution from the crystalline references (shown in Figure S4), peak A can be associated with Cu^{2+} and peak B with Cu^{+} species. Depending on the point of interest, there are important variations in the relative intensities of peaks A and B. Furthermore, Cu^{2+}'s peak A is more prevalent in sample 62 than in sample 25, regardless of the point of measurement, whereas the intensity of Cu^{+}'s peak B is comparable in both samples. This difference between the two samples indicates that the Cu^{2+}/Cu^{+} ratio leans more toward Cu^{+} in sample 25 than in sample 62.

The dotted curves in both Figure 5a,b show the subtraction between a spectrum recorded in an orange band and a spectrum recorded in a red band. The same shape is obtained by this operation on the other red and orange bands. Positive features indicate an intensity increase in the orange spectrum compared to the red spectrum.

We note that the Cu^{2+} peak A does not vary in the same way for samples 25 and 62. The difference spectrum exhibits a negative contribution for sample 25, while it shows a raise in intensity for sample 62. This difference in behaviour shows that the proportion of remaining Cu^{2+} in sample 25 is reduced in the orange stripes. In contrast, the proportion of Cu^{2+} is increased in the orange stripes of sample 62.

Secondly, a wavy feature (positive then negative) around 935 eV is present in both samples. This indicates that the position of peak B in spectra measured in orange parts is at lower energies, suggesting a change in the environment around the Cu^{+} ions. The peak B position for the points measured in the orange zones are close to that on the XANES spectrum of cuprite (Figure 5a). This peak is also broad and asymmetric, as observed for cuprite. The evolution in the position of peak B can thus differentiate Cu^{+} in the glass part (red zones) at high energy from Cu^{+} in cuprite crystals (orange zones) at low energy.

In the red parts for both samples, peak B does not show any contribution of crystalline copper, either cuprite or metallic copper. This reveals that the size of the crystals or the proportion of crystallized copper in the red parts is too low to show a significant contribution to the XANES signal.

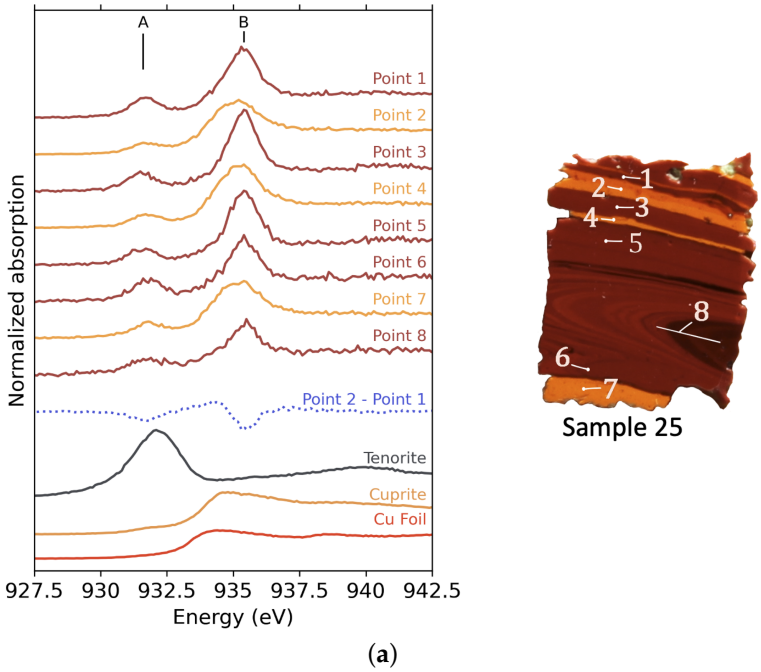

(**a**)

Figure 5. *Cont.*

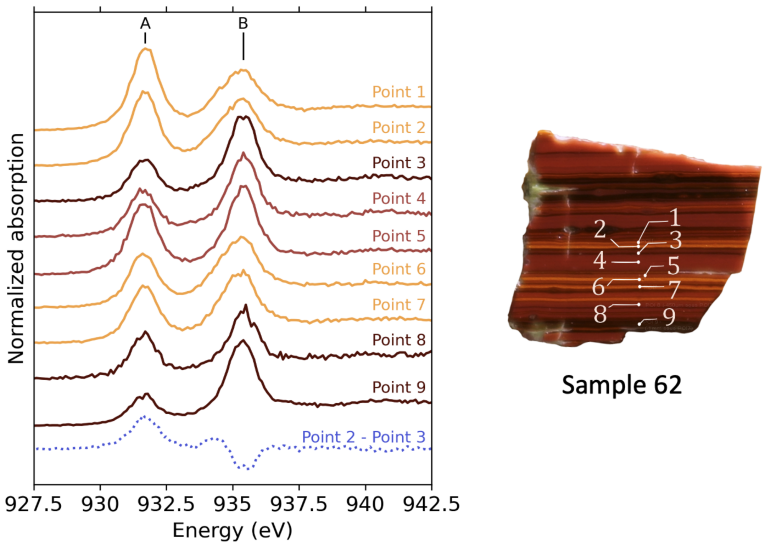

(**b**)

Figure 5. XANES spectra at the Cu L_3-edge of selected points in the striped tesserae. The colour of the curves represents the colour of the selected point. The blue dotted curve is the difference spectrum between spectra measured in orange and red zones. (**a**) XANES spectra for sample 25 and images showing the points of measurement. For point 8, the beam was defocussed, and the line indicates the size of the beam. (**b**) XANES spectra for sample 62 and images showing the points of measurement.

3.2.3. Microstructure

Figures 6 and 7 present SEM images of sample 25 and 62, showing the similarities and differences of the crystallisation behaviour occurring in the two types of stripes (red and orange). The light and dark grey bands correspond to density contrast, mainly due to differences in lead and copper contents. Dark regions are those with lower lead and copper, and they correspond to red stripes. The size and surface density of particles measured by image threshold are presented in Table 3. In both samples, zones are observed at the interface between the stripes that are completely depleted of crystals. This is visible in the upper right-hand corner of Figure 6d and in the upper and lower regions of Figure 7b (white arrows). These crystal-free regions are also the boundaries between the areas that show different contrasts, corresponding to the dense (high lead and high copper) glass shown by a light grey, and the less dense one, shown by a darker grey. In sample 62, this crystal depletion tends to correspond to streaks of a darker red colour that are also opaque.

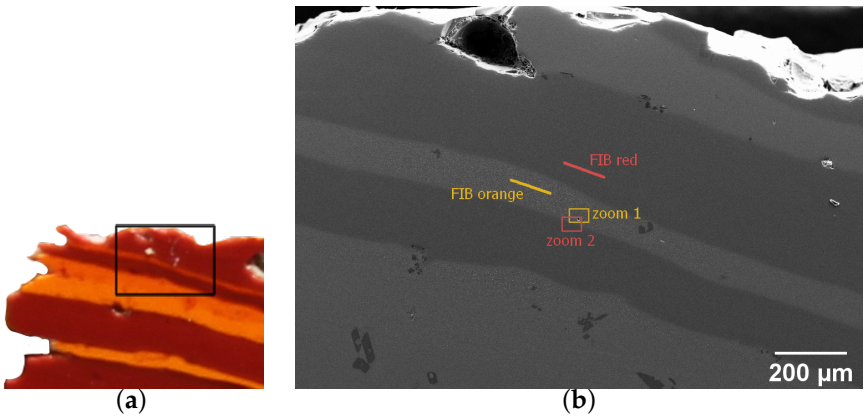

(**a**) (**b**)

Figure 6. *Cont.*

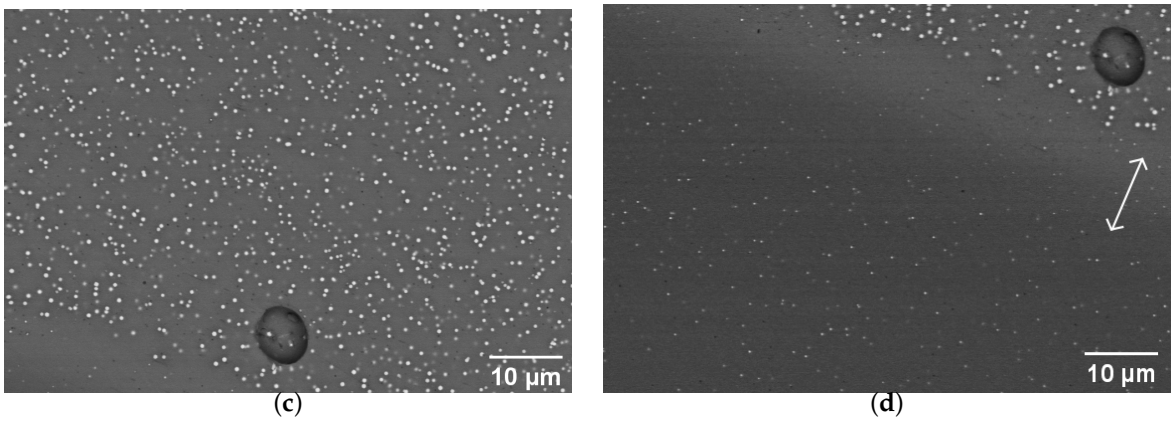

(**c**) (**d**)

Figure 6. SEM imaging of striated tessera 25. (**a**) Photo of the tessera showing the probed region, given by the black rectangle. (**b**) Large view of the studied zone. The lines indicate the positions of FIB sample preparations for TEM imaging, presented in Figure 8. The rectangles indicate the positions of images shown in (**c**,**d**). (**c**) View of the orange stripe of (**b**) (zoom 1). (**d**) View of a red stripe (zoom 2). The spherical object is the same air bubble in both (**c**,**d**). The arrow indicates a zone of particle depletion at the colour boundary.

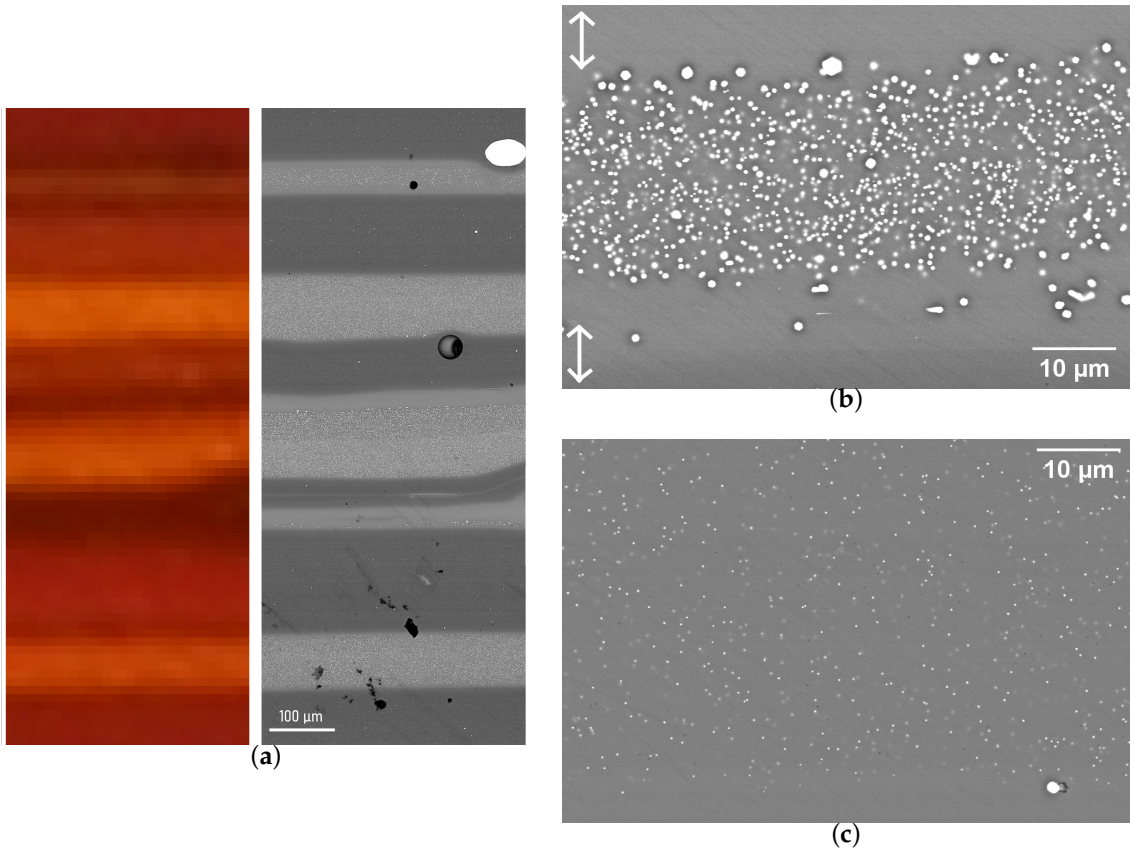

(**a**) (**b**) (**c**)

Figure 7. SEM imaging of striped tessera 62. (**a**) Large view of the studied zone. The light and dark grey stripes correspond to density contrast, mainly given by differences in lead content. (**b**) View of an orange stripe. The white arrows show particle depletion at the stripe boundaries. (**c**) View of a red stripe.

Table 3. Size and number density analysis of the SEM images presented in Figures 6 and 7.

	Max Diameter (nm)	Mean Diameter (nm)	Half-Heigh Width (nm)	Surface Number Density ($particle \cdot \mu m^{-2}$)
Sample 25				
Red zone	620	300		0.045
Orange zone	800	490	270	0.26
Sample 62				
Red zone	450	300	60	0.18
Orange zone	2030	450	200	0.54

TEM analyses of two thin sections taken from sample 25 are shown in Figure 8a,b. A clear difference in the shapes and sizes of the particles can be observed in the two regions. The crystals in the orange zone are large (with sizes matching those determined in the SEM analysis) and are faceted hexagons. The red part also contains crystals, the size of which matches the SEM images, but which are almost perfectly spherical, with only a slight hint of facets. SAED carried out on single particles reveal the presence of cuprite Cu_2O particles in orange regions (Figure 8c) and small metallic Cu in red regions (Figure 8d).

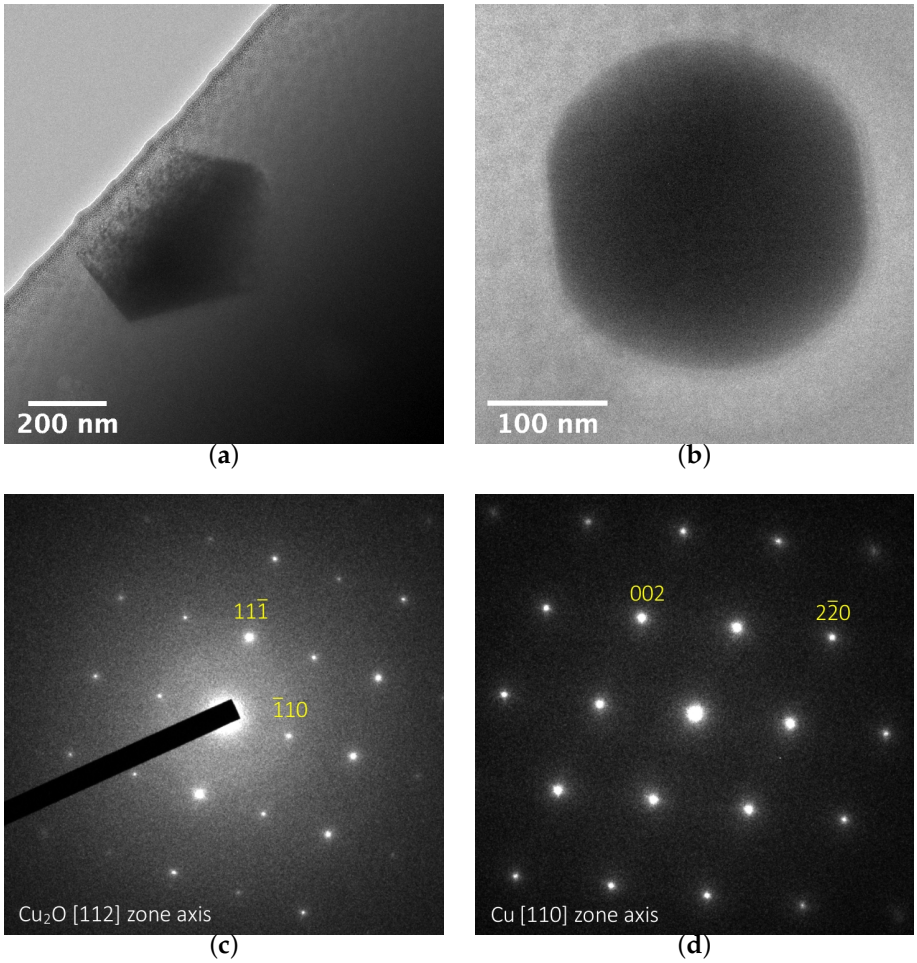

Figure 8. TEM bright field images (**a**) in the orange zone and (**b**) in the red zone of sample 25. Diffraction patterns are shown of crystals (**c**) in the orange zone and (**d**) in the red zone. The location of the fine slice sampling is shown in the large view in Figure 6d.

4. Discussion

4.1. Compositional Classification of Red/Orange Glasses/Tesserae

The variability in colour in the selected tesserae is mirrored in the variability of the compositions, especially in terms of the copper and lead content. In the monochrome tesserae, the brown-red samples have low copper and low lead contents, while the orange ones have high copper and high lead contents (Table S1). There is also compositional variability within the same sample, resulting in red and orange stripes. However, the lead content in the orange stripes is much lower than in the monochrome orange sample (Tables 2 and S1).

Ancient red and orange opaque glasses are usually classified as two main groups [17,20], with a few outliers (Figure 9).

- Low-copper (CuO < 4 wt%) and low-lead (PbO < 10 wt%);
- High-copper (5–12 wt% CuO) and high-lead (20–40 wt% PbO).

In the first compositional field, opaque red and brown-red samples are often described. The colouration is due to spherical or cubic metallic copper nanoparticles by a surface plasmon resonance effect (Figure S5). The final hue depends on the size and concentration of nanoparticles, and the strong colouring power opacifies a sample only a few millimeters thick. The size of the crystals typically ranges between 50 and 500 nm in diameter [41] or even bigger for the browner hue (1 µm) [18]. The colouration of samples 14 and 29 is consistent with this description, with sample 29 in the upper range of lead concentrations, and sample 14 at the lower-copper lower-lead range. Both are coloured by metallic copper nanoparticles, with sizes similar to those encountered in the literature (300 nm for sample 25). In previous works [13,20], examples of red glasses coloured by metallic copper having less than 3 wt% of copper but 15 to 25 wt% of lead are described, but they remain atypical. Lead is thought to have little influence on the precipitation of metallic copper [23], which may explain why such compositions are rare.

The second category (high-lead high-copper) results in several colours ranging from yellowish-orange, red-orange to bright "sealing wax" red. All of them are due to cuprite crystals, although some are reported to have been found with a minority of metallic copper particles mixed in. The colouration by cuprite crystals is due to the energy band gap (Figure S5), nominally at 2.1 eV [42]. The crystal size and shape affect the final hue, and the orange colour is favoured by small cuprite crystals. The sealing wax colouration is often described as much brighter than the Cu^0 brown-red one [17,43], but Bandiera et al. [18] have shown that some Cu^0 colourations are as bright as sealing wax red, undistinguishable to the naked eye, especially when the iron content is low. The two orange monochrome samples that we have analysed fit into this compositional category but with somewhat lower lead concentration of 17 wt% for sample 70.

The red parts of the striated tesserae are in the low-copper and low-lead group, with nanometric metallic copper crystals colouring them red to brown-red. However, the orange stripes cannot be classified in any of the two groups previously described. In fact, while they have high copper contents (CuO > 10 wt%), they have way less lead than the high-copper and high-lead category proposed by Freestone: the lead content of the orange zones is below 12 wt% PbO in sample 25 and even below 3 wt% PbO in sample 62. Even if most cuprite coloured glasses, especially Roman ones, have very high lead contents, the exception to that rule deserves special attention. In fact, previous studies have shown that lead is not necessary to produce orange and red cuprite colours [15,23]. Some authors also described glasses coloured by cuprite with lead content below 10 wt% [14], including Roman glasses [20]. This type of composition is often overlooked when categorizing the possible type of copper red and orange. Based on our analysis and previous studies, we can propose an additional group to take into account when considering copper red and orange:

- High-copper (5–15 wt% CuO) and low- to medium-lead (<13 wt% PbO).

This may seem an arbitrary cut-off between the high-lead and the low-lead groups with high copper content, but such separate categories are useful to distinguish the compositions

that have skyrocketing amounts of lead (up to 36 wt% in [22]) from those, such as the present striated samples, with medium to low lead content. This distinction is also useful as the lead content influences the cuprite crystal habitus and thus the colour (see below).

These two high copper content categories make it clear that cuprite formation is mainly favoured by the copper abundance, even though the presence of lead promotes the formation of cuprite and, more specifically, its crystalline growth.

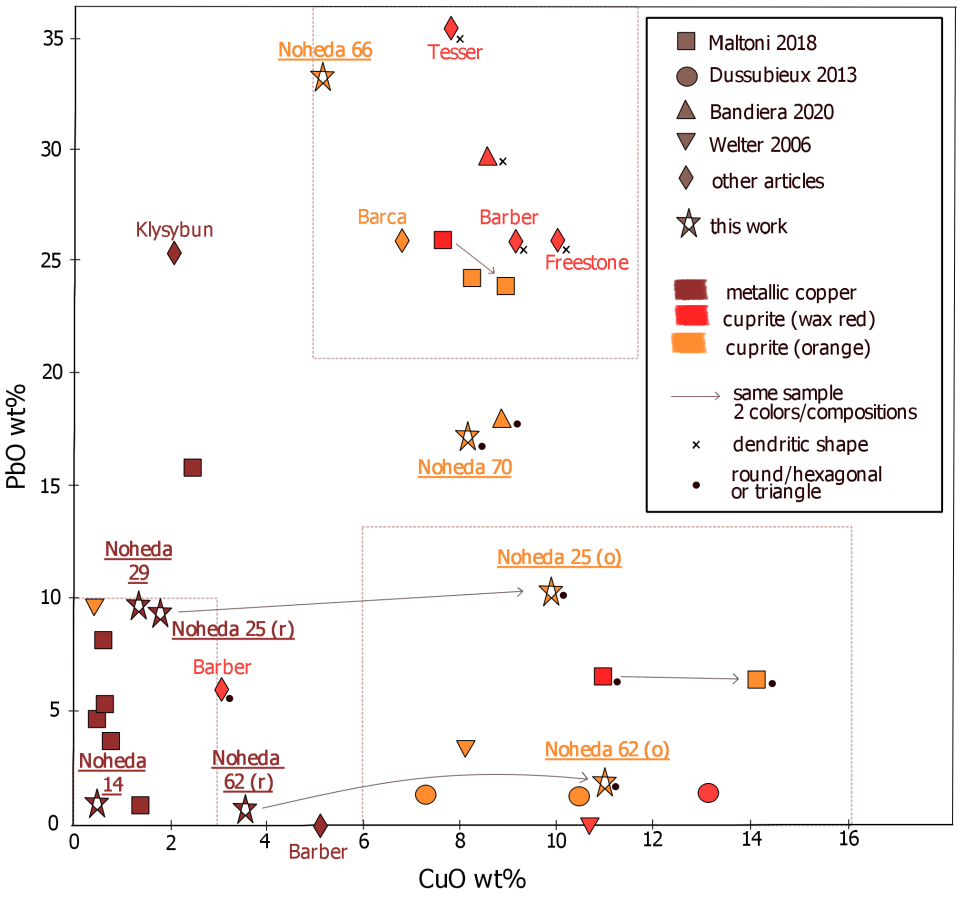

Figure 9. Review of copper and lead contents in archaeological samples, with information on the colouring particles and their shape, when avalaible [12–15,18,20,22,23,43].

4.2. Role of Lead in the Colour Formation

Several hypotheses about the role of lead in the promotion of cuprite colours have been formulated in the literature [10,43]. It has been proposed that lead may increase the solubility of copper in the melt, or favour the solubility of Cu^{+} relative to Cu^{2+}. However, examples of high copper contents in low-lead glasses, exceeding the Cu content in high-lead glasses ([20], over 14 wt% of copper), invalidate the solubility hypothesis. Edward et al. [44] have found an increase in the Cu^{+}/Cu^{2+} ratio with lead addition, and Ahmed et al. observed the increase in Cu_2O precipitation [43]. However, rather than an effect on Cu^{+} solubility, these studies indicate that the addition of lead has a reducing influence on the copper redox speciation. A recent thermodynamic study [45] has shown that high lead concentration favours cuprite precipitation, but the region in SiO_2-Cu_2O-PbO ternary diagram corresponding to our tesserae compositions is not in the crystallisation field of cuprite (Figure S6). This way, lead may have little influence thermodynamically on cuprite crystallisation.

Another interesting hypothesis is that Pb is added to help the growth of cuprite crystals and to thus tune the colouration. Lead, in fact, lowers the viscosity of the melt [10], which could prevent the crystallization of the silicate phases at temperatures that must be reached

for a certain time to promote the growth of cuprite crystals, necessary to obtain the sealing wax colouration. The differences in cuprite colours are due to different sizes of the cuprite crystals. As shown by Ahmed et al. [9], small crystals cause orange or even yellow, whereas the bigger ones produce red.

In the literature, all examples of cuprite crystals that are larger than 1 µm and that form characteristic dendritic shapes are found in glasses with very high lead content (above 25 wt%), giving bright red colouration (Figure 9). The width of the branches in these dendrites are micrometric (1–2 µm), and the dendrites themselves reach 50–150 µm [12,22,41,43]. Furthermore, orange colouration occurs more frequently (and red less frequently) in the third group (low to medium lead, high copper contents). Additionally, up to 18 wt% lead, the orange samples are not coloured by Cu_2O crystals with dendritic habitus but rather by spherical or hexagonal Cu_2O crystals, ranging in size from 100 nm to 1 µm (samples 25 and 62 orange parts and sample 70, and Bandiera et al. [18]). Some pre-Roman red glasses with negligible or very low lead levels are also coloured by cuprite particles [14,15], which are bigger (1.5–2.5 µm) than in the orange-coloured samples examined here; however, they are not dendritic but rather spherical or slightly elongated [15].

The lead content thus seems to be a crucial parameter for the final shape of cuprite crystals and, in particular, for the growth of dendritic crystals that is required for the production of sealing wax red. As an additional benefit, lead enhances the brilliance and soften the glass, which facilitates its cutting [21].

4.3. Reducing Agents

It is notable that MgO and K_2O concentrations in the striped samples are above 1.5 wt% (Table 2). This is a typical feature of all orange and some red samples from Noheda [24]. This specificity is often described for copper red glasses or tesserae [14,20,21,41,43], and Fiori et al. [25] reports it to be more frequent in low-lead and low-copper glasses (first group). High magnesia and potash contents indicate either the use of sodium-rich plant ashes [14] or the addition of an ash component to a natron glass [20,24]. According to Maltoni et al. [20], plant ashes added to a pre-existing glass could act as a reducing agent because of the residual carbon it contains.

The concentration of FeO exceeding 1.2 wt% is above the content expected from contamination from the glass raw materials [23]. The iron content is slightly higher in the orange bands compared to the red ones in the striped tesserae (Table 2). Similarly, the Sn content is higher in the orange bands than in the red ones. These two elements, Fe and Sn, are well known to act as reducing agents for copper favoring the formation of Cu^+ or Cu^0. However, their concentration is low and insufficient to bring a technical benefit as internal reducing agents. Most probably, their presence is not intentional as they enter the batch as impurities, together with the copper raw materials such as bronze [23,46,47], or together with lead in the form of a lead-tin alloy such as pewter [25]. The use of bronze or pewter as raw materials is supported by the compositional correlations of Cu, Pb and Sn in all the previously studied red and orange samples from this site, shown in Figure S7.

4.4. Technological Implications

One of the major results of our SEM-EDX and XANES analysis concerns the striated tesserae. In all the samples studied here, some level of striation is observed. It can be seen either at the microscopic level (samples 70 and 29) or clearly obvious as macroscopic stripes (samples 25 and 62).

To our knowledge, no example of Cu^0 and Cu_2O forming stripes within the same samples was previously reported in literature. Among the various stripes in tesserae previously reported, yellow-orange and red-orange stripes differ in the size of cuprite crystals with either no compositional differences [18] or with higher copper content in the lighter bands [20]. Brown-red and red stripes have been attributed to varying sizes of metallic copper nanocrystals [18], with darker stripes associated with a high iron content [20]. Red (Cu^0)/colourless stripes [18] as well as red (Cu^0)/black and orange (Cu_2O)/black were

also reported [21], with no particles detected in the colourless and in the black bands. In short, according to these previously published data, the striation is caused exclusively by the number and size of the crystals.

Conversely, our XANES and SEM/TEM analysis reveal that the nature of the colouring crystals is different in the red (Cu^0) and orange (Cu_2O) bands of the same sample (25 and 62). Additionally, the compositional difference between the stripes is larger than in previous works as we reveal higher Cu and Pb (and slightly higher Fe and Sn) contents in the orange bands compared to the red ones. Interestingly, the base glass composition (Table 2) for the different stripes is similar, which indicates that the same glass is used for the red and orange.

It is unclear if the orange/red striped tesserae were produced on purpose or accidentally. However, they are abundant in Roman and Byzantine mosaics and they were likely intentionally used by glass-makers due to their aesthetic aspects. For instance, Tesser and Verità [22] described polychrome 2nd-century Roman glasses used to imitate exotic marbles. The imitation of *cipollino rosso* especially is a mix of two glasses fused together: white and Cu^0 red. It is thus likely that, to achieve the polychrome red and orange striped tesserae of Noheda, two batches were voluntarily mixed together with one previously enriched in copper and lead; the stirring of the molten glasses caused the alternating bands.

Still, it is remarkable that the glassmakers could have good enough control over the reducing conditions of the furnaces to produce both Cu^0 and Cu_2O within the same sample. Since the colourations are created by in situ precipitation of copper and copper oxide, re-melting the glass is risky. Nanoparticles can dissolve rapidly when the molten glass comes in contact with air, resulting in a loss of red/orange colours. For lower temperatures, the cuprite growth can restart, giving a red colouration. To maintain both red and orange when mixing two glasses requires good control of the oxygen partial pressure (reducing conditions) of the furnace atmosphere. Charcoal and plant ashes can be added to create these suitable reducing conditions [25], which may explain the high magnesia and potash content in these tesserae. The control of the furnace atmosphere should operate in a narrow range of reducing conditions to allow the precipitation and growth of copper or cuprite crystals. However the reduction should not be too strong to avoid the precipitation of too many metallic particles, which tend to degrade the colour towards brown or black [10,25]. A red band rich in lead is observed in sample 25 (Figure 4) that could arise from lead diffusion from the orange part. This zone indicates uneven mixing between the two glasses that implies a short duration of melting. Thereby, the alternating red/orange bands result from a control of the reducing conditions in the furnace, the melting time and glass compositions, reflecting the high technical expertise of the glassmakers. In archaeological samples, composition and microstructure can be investigated, but firing conditions are harder to decipher. To truly understand the manufacturing processes, a reproductive approach is needed.

5. Conclusions

We have investigated six red and orange opaque glass tesserae using XANES spectroscopy and electron microscope imaging. This allowed us to identify metallic copper nano-particles in the brown-red samples, while the orange glasses were coloured by copper oxide Cu_2O nanoparticles with remaining Cu^+ in the glass. The orange samples had higher Cu concentrations. Compositional analysis revealed that the same base glass was used in the red and orange bands of the two studied banded samples with addition of Cu, Sn, Pb and probably Fe. The red hues, present in both monochrome and banded tesserae, corresponded to a low-copper and low-lead group frequently described in the literature. In monochrome and banded samples coloured by cuprite, there was variability in composition, especially regarding the copper and lead contents. Based on these differences and on our literature review, we propose a high-copper/low-lead group to account for the variability in composition. The addition of plant ash to the glass batch as a reducing agent is probable.

Supplementary Materials: The following materials are available online at www.mdpi.com/xxx/s1. Figure S1: X-ray diffractograms (Co anode) of the studied tesserae; Figure S2: Linear combination fitting of XANES spectra at Cu K-edge of monochrome tesserae; Figure S3: SEM images with AsB detection of undissolved raw material in sample 25 (a) in an orange area and (b) in a red area; Figure S4: XANES spectra at Cu L3-edge for crystalline references; Table S1: Composition (wt%) measured by LA-ICP-MS reported from Schibille et al. [24] supplementary information; Figure S5: Optical absorption spectra measured in reflexion with integrating sphere of Noheda red and orange samples; Figure S6: Ternary diagram for SiO2-Cu2O-PbO systems in equilibrium with metallic copper [45]; Figure S7: Pairs of elements for all red and orange tesserae samples from Noheda villa, from Schibille et al. 2020 [24] Supplementary Information ([48–54]).

Author Contributions: Conceptualization, C.N. and L.C.; methodology, N.T. and E.F.; formal analysis, C.N.; investigation, C.N. and L.C.; resources, N.S.; writing—original draft preparation, C.N.; writing—review and editing, C.N., L.C., N.S., N.M., N.T. and E.F.; supervision, L.C. All authors have read and agreed to the published version of the manuscript.

Funding: This research received no external funding.

Institutional Review Board Statement: Not applicable.

Informed Consent Statement: Not applicable.

Data Availability Statement: Data are available upon request. Please contact the corresponding author.

Acknowledgments: The SEM facility at IMPMC was supported by Région Ile de France Grant SESAME 2006 NOI-07-593/R, Institut National des Sciences de l'Univers (INSU)-CNRS, Institut de Physique-CNRS, Sorbonne Université, and the French National Research Agency (ANR) grant ANR-07-BLAN-0124-0. We thank Béatrice Doisneau for the FIB elaboration and her useful suggestions and comments.

Conflicts of Interest: The authors declare no conflict of interest.

References

1. Bring, T.; Högskolan, K.T.; Kemi, O. Red Glass Coloration: A Colorimetric and Structural Study. Ph.D. Thesis, Oorganisk Kemi, KTH Kemi, Stockholm, Sweden, 2006.
2. Cãpãþînã, C. The Study of Copper Ruby Glass. *Ceram. Silikàty* **2005**, *49*, 283–286.
3. Quaranta, A.; Ceccato, R.; Pederiva, L.; Capra, N.; Dal Maschio, R. Formation of copper nanocrystals in alkali-lime silica glass by means of different reducing agents. *J. Non-Cryst. Solids* **2004**, *345&346*, 671–675. [CrossRef]
4. Cuvelier, P.A.; Andraud, C.; Chaudanson, D.; Lafait, J.; Nitsche, S. Copper red glazes: A coating with two families of particles. *Appl. Phys. A* **2012**, *106*, 915–929. [CrossRef]
5. Colomban, P.; Schreiber, H.D. Raman signature modification induced by copper nanoparticles in silicate glass. *J. Raman Spectrosc.* **2005**, *36*, 884–890. [CrossRef]
6. Wakamatsu, M.; Takeuchi, N.; Nagai, H.; Ishida, S. Chemical States of Copper and Tin in Copper Glazes Fired under Various Atmospheres. *J. Am. Ceram. Soc.* **1989**, *72*, 16–19. [CrossRef]
7. Drünert, F.; Blanz, M.; Pollok, K.; Pan, Z.; Wondraczek, L.; Möncke, D. Copper-based opaque red glasses—Understanding the colouring mechanism of copper nanoparticles in archaeological glass samples. *Opt. Mater.* **2018**, *76*, 375–381. [CrossRef]
8. Ahmed, A.A.; Ashour, G.M. Effect of melting conditions on the crystallisation of cuprous oxide and copper in glass. *Elev. Congr. Glass* **1977**, *2*, 177–187.
9. Ahmed, A.A.; Ashour, G.M. Effect of heat treatment on the crystallisation of cuprous oxide in glass. *Glass Technol.* **1980**, *22*, 24–32.
10. Cable, M.; Smedley, J.W. The Replication of an Opaque Red Glass from Nimrud. *Br. Mus. Occas. Pap.* **1987**, *56*, 151–164.
11. Vandiver, P. Glass technology at the mid-second-millenium B.C. Hurrian site of Nuzi. *J. Glass Stud.* **1982**, *25*, 239–247.
12. Barber, D.; Freestone, I.; Moulding, K. Ancient copper red glasses: Investigation and analysis by microbeam techniques. *J. Archaeol. Sci.* **2010**, *37*, 898–899. [CrossRef]
13. Klysubun, W.; Thongkam, Y.; Pongkrapan, S.; Won-in, K.; T-Thienprasert, J.; Dararutana, P. XAS study on copper red in ancient glass beads from Thailand. *Anal. Bioanal. Chem.* **2011**, *399*, 3033–3040. [CrossRef]
14. Gratuze, B.; Blet-Lemarquand, M.; Dussubieux, L. Innovation dans les techniques de coloration: Les verres rouges et orange en Asie du Sud. In *Les Cahiers de L'Institut D'histoire Sociale du Verre et de la Céramique*; IHS Verre et Céramique: Montreuil, France, 2013; pp. 11–20.
15. Welter, N.; Schüssler, U.; Kiefer, W. Characterisation of inorganic pigments in ancient glass beads by means of Raman microspectroscopy, microprobe analysis and X-ray diffractometry. *J. Raman Spectrosc.* **2007**, *38*, 113–121. [CrossRef]
16. Brun, N.; Mazerolles, L.; Pernot, M. Microstructure of opaque red glass containing copper. *J. Mater. Sci. Lett.* **1991**, *10*, 1418–1420. [CrossRef]

17. Freestone, I.C.; Stapleton, C.P.; Rigby, V. The production of red glass and enamel in the Late Iron Age, Roman and Byzantine periods. In *Through a Glass Brightly—Studies in Byzantine and Medieval Art and Archaeology Presented to David Buckton*; Entwistle, C., Ed.; Oxbow: Oxford, UK, 2003; pp. 142–154.
18. Bandiera, M.; Verità, M.; Lehuédé, P.; Vilarigues, M. The Technology of Copper-Based Red Glass Sectilia from the 2nd Century AD Lucius Verus Villa in Rome. *Minerals* **2020**, *10*, 875. [CrossRef]
19. Boschetti, C.; Henderson, J.; Evans, J. Mosaic tesserae from Italy and the production of Mediterranean coloured glass (4th century BCE—4th century CE). Part II: Isotopic provenance. *J. Archaeol. Sci. Rep.* **2017**, *11*, 647–657. [CrossRef]
20. Maltoni, S.; Silvestri, A. A Mosaic of Colors: Investigating Production Technologies of Roman Glass Tesserae from Northeastern Italy. *Minerals* **2018**, *8*, 255. [CrossRef]
21. Santagostino Barbone, A.; Gliozzo, E.; D'Acapito, F.; Memmi Turbanti, I.; Turchiano, M.; Volpe, G. The Sectilia Panels of Faragola (Ascoli Satriano, Southern Italy): A Multi-Analytical Study of the Red, Orange and Yellow Glass Slabs. *Archaeometry* **2008**, *50*, 451–473. [CrossRef]
22. Tesser, E.; Verità, M.; Lazzarini, L.; Falcone, R.; Saguì, L.; Antonelli, F. Glass in imitation of exotic marbles: An analytical investigation of 2nd century AD Roman sectilia from the Gorga collection. *J. Cult. Herit.* **2020**, *42*, 202–212. [CrossRef]
23. Barca, D.; Basso, E.; Bersani, D.; Galli, G.; Invernizzi, C.; La Russa, M.F.; Lottici, P.P.; Malagodi, M.; Ruffolo, S.A. Vitreous tesserae from the calidarium mosaics of the Villa dei Quintili, Rome. Chemical composition and production technology. *Microchem. J.* **2016**, *124*, 726–735. [CrossRef]
24. Schibille, N.; Boschetti, C.; Valero Tévar, M.A.; Veron, E.; de Juan Ares, J. The Color Palette of the Mosaics in the Roman Villa of Noheda (Spain). *Minerals* **2020**, *10*, 272. [CrossRef]
25. Fiori, C. Production technology of Byzantine red mosaic glasses. *Ceram. Int.* **2015**, *41*, 3152–3157. [CrossRef]
26. Silvestri, A.; Tonietto, S.; Molin, G.; Guerriero, P. The palaeo-Christian glass mosaic of St. Prosdocimus (Padova, Italy): Archaeometric characterisation of tesserae with copper- or tin-based opacifiers. *J. Archaeol. Sci.* **2014**, *42*, 51–67. [CrossRef]
27. Shugar, A.N. Byzantine Opaque Red Glass Tesserae from Beit Shean, Israel. *Archaeometry* **2000**, *42*, 375–384. [CrossRef]
28. Adlington, L.; Ritter, M.; Schibille, N. Production and Provenance of Architectural Glass from the Umayyad Period. *PLoS ONE* **2020**, *15*, e0239732. [CrossRef]
29. Farges, F.; Etcheverry, M.P.; Scheidegger, A.; Grolimund, D. Speciation and weathering of copper in "copper red ruby" medieval flashed glasses from the Tours cathedral (XIII century). *Appl. Geochem.* **2006**, *21*, 1715–1731. [CrossRef]
30. Kunicki-Goldfinger, J.J.; Freestone, I.C.; McDonald, I.; Hobot, J.A.; Gilderdale-Scott, H.; Ayers, T. Technology, production and chronology of red window glass in the medieval period—Rediscovery of a lost technology. *J. Archaeol. Sci.* **2014**, *41*, 89–105. [CrossRef]
31. Li, Y.; Yang, Y.; Zhu, J.; Zhang, X.; Jiang, S.; Zhang, Z.; Yao, Z.; Solbrekken, G. Colour-generating mechanism of copper-red porcelain from Changsha Kiln (A.D. 7th–10th century), China. *Ceram. Int.* **2016**, *42*, 8495–8500. [CrossRef]
32. Maxwell, M.J. The Reception and Adaptation of Oriental Ceramics in Britain, with Particular Reference to Imperial Chinese Copper—Red Wares. Ph.D. Thesis, University of Glasgow, Glasgow, UK, 2017.
33. Peak, J.R.N. Early Anglo—Saxon Glass Beads: Composition and Origines Based on the Finds from RAF Lakenheat, Suffolk. Ph.D. Thesis, Cardiff University, Cardiff, UK, 2013.
34. Lilyquist, C.; Brill, R. *Studies in Early Egyptian Glass*; The Metropolitan Museum of Art: New York, NY, USA, 1993.
35. Fonda, E.; Rochet, A.; Ribbens, M.; Barthe, L.; Belin, S.; Briois, V. The SAMBA quick—EXAFS monochromator: XAS with edge jumping. *J. Synchrotron Radiat.* **2012**, *19*, 417–424. [CrossRef]
36. Bearden, J.A.; Burr, A.F. Reevaluation of X-ray Atomic Energy Levels. *Rev. Mod. Phys.* **1967**, *39*, 125–142. [CrossRef]
37. Ravel, B.; Newville, M. *ATHENA ARTEMIS HEPHAESTUS*: Data Anal. X-Ray Absorpt. Spectrosc. Using *IFEFFIT*. *J. Synchrotron Radiat.* **2005**, *12*, 537–541. [CrossRef]
38. Vantelon, D.; Trcera, N.; Roy, D.; Moreno, T.; Mailly, D.; Guilet, S.; Metchalkov, E.; Delmotte, F.; Lassalle, B.; Lagarde, P.; et al. The LUCIA beamline at SOLEIL. *J. Synchrotron Radiat.* **2016**, *23*, 635–640. [CrossRef]
39. Thakur, P.; Bisogni, V.; Cezar, J.C. Electronic structure of Cu-doped ZnO thin films by X-ray absorption, magnetic circular dichroism, and resonant inelastic X-ray scattering. *J. Appl. Phys.* **2010**, *107*, 103915 [CrossRef]
40. Rothe, J.; Hormes, J.; Bönnemann, H.; Brijoux, W.; Siepen, K. In Situ X-ray Absorption Spectroscopy Investigation during the Formation of Colloidal Copper. *J. Am. Chem. Soc.* **1998**, *120*, 6019–6023. [CrossRef]
41. Bandiera, M.; Lehuédé, P.; Verità, M.; Alves, L.; Biron, I.; Vilarigues, M. Nanotechnology in Roman Opaque Red Glass from the 2nd Century AD. Archaeometric Investigation in Red Sectilia from the Decoration of the Lucius Verus Villa in Rome. *Heritage* **2019**, *2*, 2597–2611. [CrossRef]
42. Malerba, C.; Biccari, F.; Leonor Azanza Ricardo, C.; D'Incau, M.; Scardi, P.; Mittiga, A. Absorption coefficient of bulk and thin film Cu_2O. *Sol. Energy Mater. Sol. Cells* **2011**, *95*, 2848–2854. [CrossRef]
43. Freestone, I.C. Composition and Microstructure of Early Opaque Red Glass. *Br. Mus. Occas. Pap.* **1987**, *56*, 173–191.
44. Edward, R.; Paul, A.; Douglas, R. Spectroscopy and oxidationreduction ofiron and copper inNa20-PbO-Si02 glasses. *Phys. Chem. Glasses* **1972**, *13*, 131.
45. Shevchenko, M.; Jak, E. Experimental Liquidus Studies of the Binary Pb-Cu-O and Ternary Pb-Cu-Si-O Systems in Equilibrium with Metallic Pb-Cu Alloys. *J. Phase Equilibria Diffus.* **2019**, *40*, 671–685. [CrossRef]

46. Brill, D.R.; Cahill, N. A Red Opaque Glass from Sardis and Some Thoughts on Red Opaques in General. *J. Glass Stud.* **1988**, *30*, 16–27.
47. Shortland, A.J.; Eremin, K. The Analysis of Second Millenium Glass from Egypt and Mesopotamia, Part 1: New WDS Analyses. *Archaeometry* **2006**, *48*, 581–603. [CrossRef]
48. Grioni, M.; Goedkoop, J.B.; Schoorl, R.; de Groot, F.M.F.; Fuggle, J.C.; Schäfers, F.; Koch, E.E.; Rossi, G.; Esteva, J.-M.; Karnatak, R.C. Studies of copper valence states with CuL3x-ray-absorption spectroscopy. *Phys. Rev. B* **1989**, *39*, 1541–1545. [CrossRef]
49. Tanaka, Y.; Karppinen, M.; Lee, J.M.; Liu, R.S.; Chen, J.M.; Yamauchi, H. Systematic Cu L2,3-edge and O K -edge XANES spectroscopy study on the infinite-layer superconductor system, (Sr,La)CuO_2. *Solid State Commun.* **2008**, *147*, 370–373. [CrossRef]
50. Meulenberg, R.W.; van Buuren, T.; Hanif, K.M.; Willey, T.M.; Strouse, G.F.; Terminello, L.J. Structure and Composition of Cu-Doped CdSe Nanocrystals Using Soft X-ray Absorption Spectroscopy. *Nano Lett.* **2004**, *4*, 2277–2285. [CrossRef]
51. van der Laan, G.; Pattrick, R.; Henderson, C.; Vaughan, D. Oxidation state variations in copper minerals studied with Cu 2p X-ray absorption spectroscopy. *J. Phys. Chem. Solids* **1992**, *53*, 1185–1190. [CrossRef]
52. Lafait, J.; Berthier, S.; Andraud, C.; Reillon, V.; Boulenguez, J. Physical colors in cultural heritage: Surface plasmons in glass. *Comptes Rendus. Phys.* **2009**, *10*, 649–659. [CrossRef]
53. Huang, J.-Y.; Madasu, M.; Huang, M.H. Modified Semiconductor Band Diagrams Constructed from Optical Characterization of Size-Tunable Cu_2O Cubes, Octahedra, and Rhombic Dodecahedra. *J. Phys. Chem. C* **2018**, *122*, 13027–13033. [CrossRef]
54. Thoka, S.; Lee, A.-T.; Huang, M.H. Scalable Synthesis of Size-Tunable Small Cu_2O Nanocubes and Octahedra for Facet-Dependent Optical Characterization and Pseudomorphic Conversion to Cu Nanocrystals. *ACS Sustain. Chem. Eng.* **2019**, *7*, 10467–10476. [CrossRef]